1 Global spatially-distributed sectoral GDP map for disaster risk

2 analysis

- 3 Takeshi Shoji^{1,2}, Kiyoharu Kajiyama², Dai Yamazaki^{1,2}, Yuki Kita^{2,3}, Megumi Watanabe^{2,4}
- ⁴ Graduate School of Engineering, The University of Tokyo, Tokyo, 113-8656, Japan
- ⁵ Institute of Industrial Science, The University of Tokyo, Tokyo, 153-8505, Japan
- 6 ³Gaia Vision Inc., Tokyo, Japan
- 7 ⁴LERMA, Observatoire de Paris, Paris, 75014, France
- 8 Correspondence to: Takeshi Shoji (tshoji@rainbow.iis.u-tokyo.ac.jp)
- 9 Abstract. Global risk assessments of economic losses by natural disasters while considering various land uses is essential. 10 However, sector-specific, high-resolution pixel-level economic data are not yet available globally to assess exposure to local 11 disasters such as floods. In this study, we employed new land-use data to construct global, spatially distributed map of 12 sector-specific gross domestic product (GDP). We developed three global GDP maps, SectGDP30, in 2010, 2015, and 2020 13 for service, industry, and agriculture sector with 30 arcsec resolution. Firstly, we found that the spatial relationship between 14 the distribution of industrial GDP and urban areas, where the service GDP is highly concentrated, varies across countries. 15 For example, in the United States, industrial GDP is widely dispersed regardless of urban areas, whereas in India, industrial 16 GDP is concentrated in proximity to urban areas. Secondly, we evaluated the GDP map by subnational regional statistics of 17 Thailand, where validation data are accessible. Traditional GDP maps relying solely on population distribution exhibited 18 63.0% relative error of the sectoral GDP in each subnational region to regional statistical data, which the new sector-specific 19 GDP map reduced to 26.2%. Subsequently, we assessed the map in conjunction with sector-level business interruption (BI) 20 losses resulting from river flooding. Our estimation of sector-level losses revealed that the sectoral ratio to the total loss 21 varied significantly depending on the spatial distribution of flood hazards. The estimated total loss became closer to the 22 reported value when the new GDP map was used, while sectoral ratios of losses still had some differences from the reported 23 ratios suggesting the need for further improving the procedures of loss-estimation models.—The map (SectGDP30) 24 demonstrates strong consistency ($R^2 > 0.9$) with actual sub-national statistical data, exhibiting superior alignment compared 25 to conventional GDP maps (PB-method) reliant solely on gridded population information. The methodology refined GDP 26 distribution for specific sectors. Industry GDP was more accurately mapped using non-residential land areas as a proxy, 27 effectively capturing its localized concentrations. Agriculture GDP's accuracy improved by incorporating cropland data and a 28 distance-based distribution assumption from population agglomeration. Application of this dataset in estimating 29 flood-induced business interruption (BI) losses confirmed the map's capacity to represent inter-sectoral differences in

30 estimated losses, reflecting varied hazard spatial distributions. This underscores the importance of considering sector-specific 31 spatial patterns for accurate disaster damage assessment. These maps serve as a foundational tool for estimating detailed, 32 sector-classified economic losses, enabling precise calculation of sector-specific impacts from diverse natural disasters 33 worldwide. These global sectoral GDP maps (SectGDP30) are available at 34 https://doi.org/10.5281/zenodo.1577401710.5281/zenodo.13991673 (Shoji et al., 20254).

35 1 Introduction

36 In recent years, as natural disasters have become more frequent and found throughout the world (IPCC, 2012), global spatial data including land use and socioeconomic information have become essential for estimating the extent of disaster damage and losses. With the increasing frequency and impact of localized natural disasters such as floods, high-resolution data capturing the spatial distribution of socioeconomic factors are essential. However, socioeconomic data published by international organizations such as the World Bank are often available only at the national or large municipal level. At the research level, economic data at the municipal level have been studied (Wenz et al., 2023); however, obtaining grid-level data at a resolution of several kilometers has been still challenging.

43

44 For example, as for the impact-assessment of flood disasters, researchers have undertaken a series of studies by spatially 45 calculating the amount of asset quantity and production activity overlapped with inundated areas, leveraging global maps. 46 Achieving this necessitates the downscaling of national-level data of economic activity, mainly gross domestic product 47 (GDP), to finer subnational or grid-based levels. This type of product by downscaling GDP is called a "spatially distributed 48 GDP map". This downscaling practice typically relies on gridded population data (Tanoue et al., 2021; Willner et al., 2018). 49 Alternatively, it has involved the assembly and interpolation of available subnational statistics (Duan et al., 2022; Kummu et 50 al., 2018) or the assumption that average building heights correlate with economic activity intensity (Taguchi et al., 2022). 51 GDP maps developed using these methods are generally created for specific purposes, such as disaster damage estimation, 52 and are therefore not typically released as standalone datasets or products. Among those that are publicly available, 53 "Downscaled gridded global dataset for gross domestic product (GDP) per capita PPP over 1990–2022" by Kummu et al. (2025), is notable. This dataset generates gridded GDP map products with resolutions ranging from 30 arcmin to 30 arcsec 55 for each year since 1990, based on sub-national statistics released by various countries and utilizing population count maps.

56

57 While these studies estimated the total amount of economic losses without considering the difference between sectors, the 58 sector-classified economic losses also need to be estimated because indirect economic losses, such as global supply chain 59 impact caused by the stoppage of production activity (Willner et al., 2018), can vary significantly depending upon the sector 60 directly affected by the flood (Sieg et al., 2019). However, spatial data of sectors by downscaling national-level data have

61 been lacking. Consequently, in the context of global studies, the estimation of sector-specific losses was achieved by 62 extrapolating the values of sectoral occupation fractions within urban area grids, as reported in the European Union, to other 63 regions (Alfieri et al., 2016; Dottori et al., 2018). Alternatively, it is assumed that specific groups of sectors experience 64 uniform damage ratios (Willner et al., 2018; Tanoue et al., 2020). These methods did not consider the different spatial 65 accumulation between each sector and each region, which could lead to the misestimation of sector-classified losses 66 (Jongman et al., 2012; Willner et al., 2018).

67

The dearth of global spatial data of the economic sector arises from the absence of worldwide maps with comprehensive land use categorizations (Wenz and Willner, 2022). While regional maps provide sectoral land use classifications, including commercial and industrial areas within urban regions (e.g., European Environmental Agency, 2017; Theobald, 2014; De Moel H et al., 2014; MLIT 2021), these classifications are conspicuously absent from global maps (e.g., Bontemps et al., 2011; Esch et al., 2017). Here we focused on the recent emergence of a global land use map featuring detailed urban area classifications (Pesaresi and Politis, 2022). This development is made possible by the application of machine learning techniques that extrapolate relationships between satellite observations and actual land uses, a methodology initially established by the data in the European Union and the United States (European Environmental Agency, 2017; Theobald, 2014) and subsequently extended to a global scale. Although this dataset facilitates a comprehensive consideration of detailed land-use patterns within urban areas worldwide, no study has yet integrated this dataset with socioeconomic data. Such integration holds the potential to pioneer a novel approach to estimating natural disaster damage accurately with sectoral classifications.

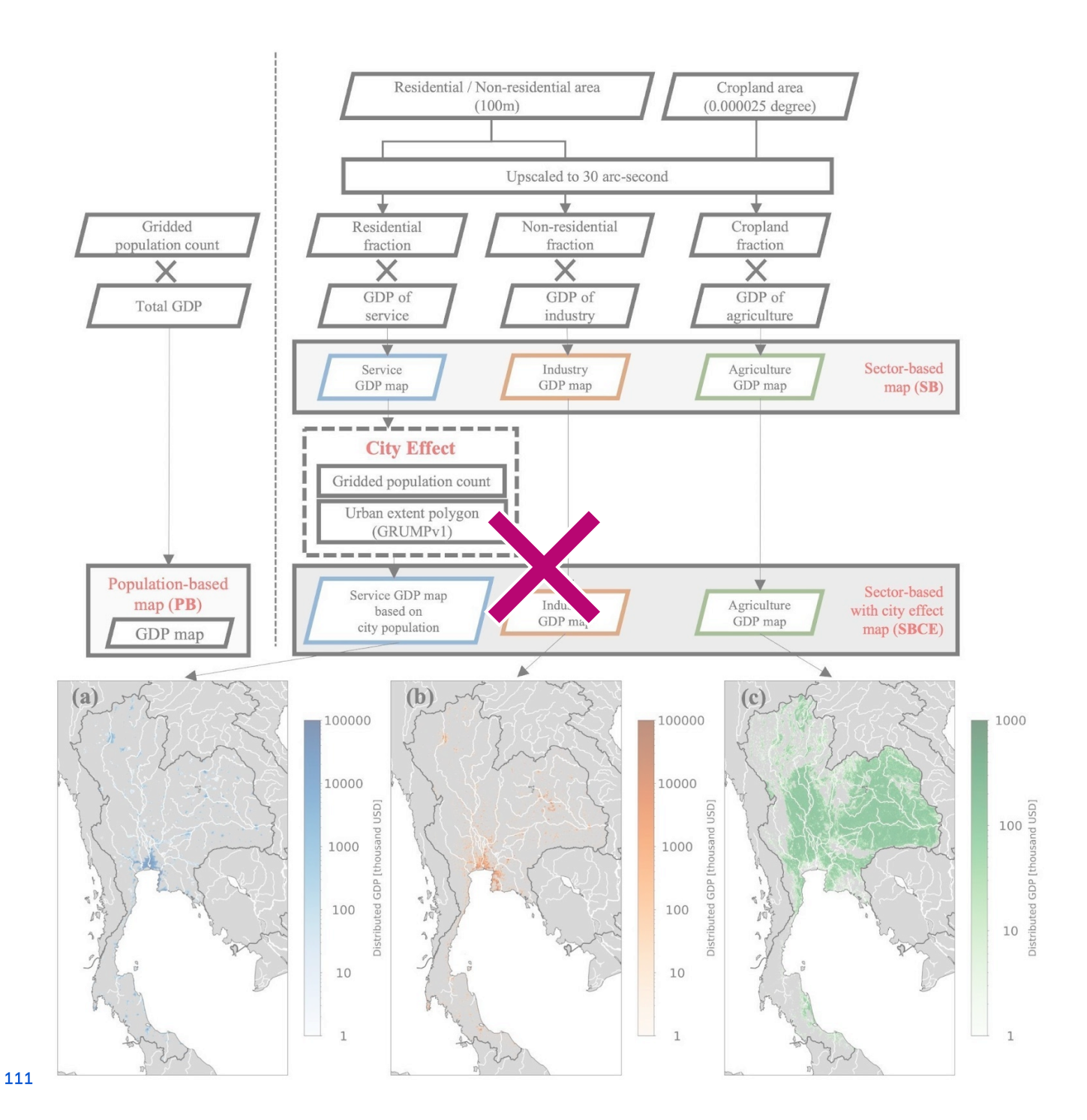
80

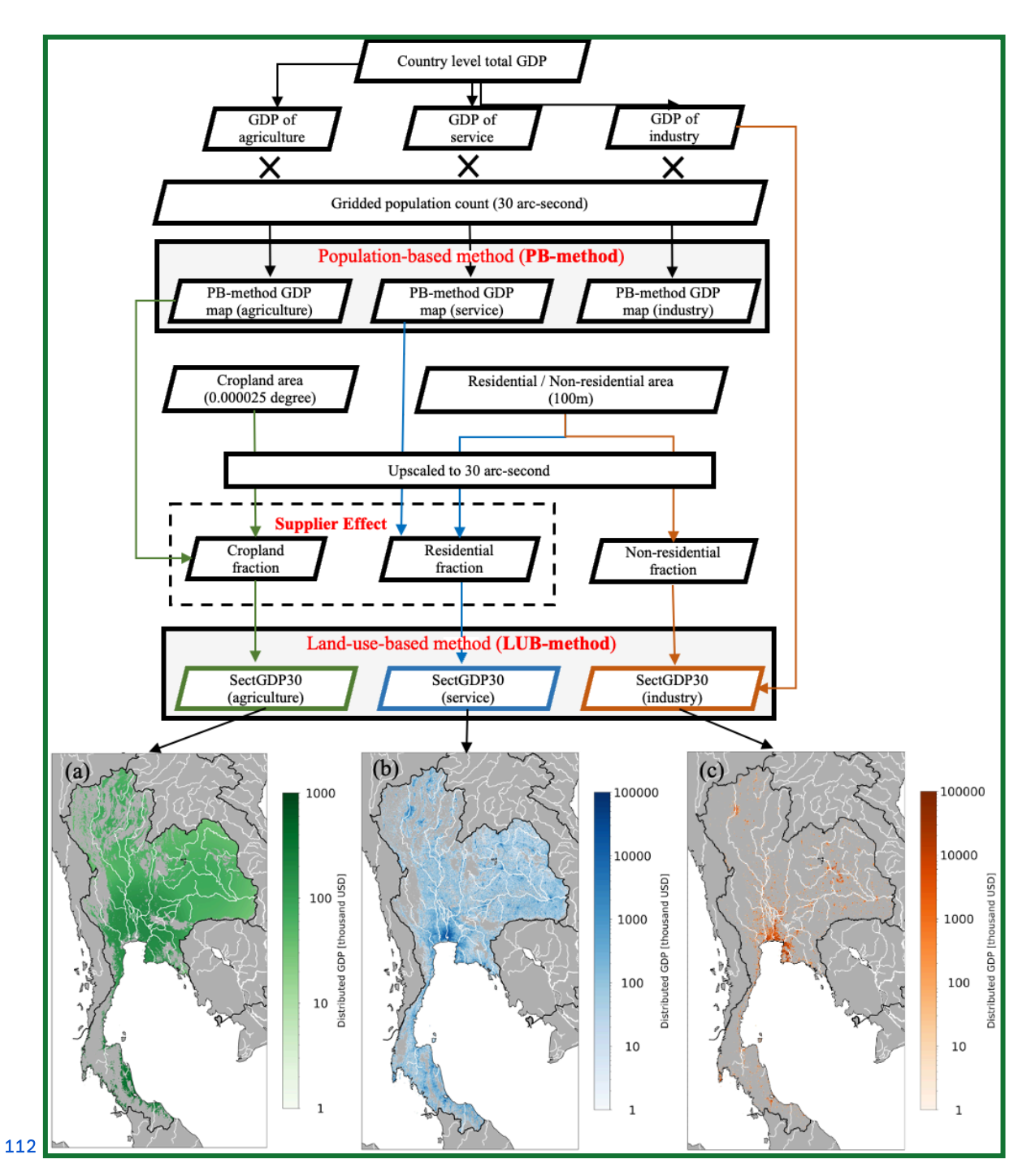
81 The objective of this study is to leverage a recently available global detailed land use map dataset to construct a spatially 82 distributed sectoral GDP map (SectGDP30). The accuracy of the GDP mapping distribution of SectGDP30 economic sectors 83 within this newly developed spatially distributed GDP map is evaluated using global sub-national scale statistics from 84 DOSE dataset (Wenz et al., 2023)data from Thailand. Validation is achieved by scrutinizing the consistency of subnational 85 statistics within Thailand. Furthermore, to discuss the applicability of SectGDP30 the new GDP map for practical economic 86 loss estimation, this study examines the estimation of business interruption losses incurred due to a flood event in Thailand 87 and compares these estimations with reported values. The reason for choosing Thailand as a target of validation was that this 88 country has both sectoral subnational GDP statistics and the reported values of sectoral economic losses caused by the 89 historical event while most countries do not have nor publish those types of data.

90 2 Methods

91 2.1 Spatially distributed sectoral GDP map

92 The spatially distributed sectoral GDP map was created in two steps (Figure 1). First, we created a global sectoral land use 93 fraction map at a spatial resolution of 30 arcsec, and combined satellite products to classify three sectors: the service, 94 industry, and agricultural sectors. Then, country GDP data classified according to these sectors were distributed spatially on 95 the corresponding sectoral area fractions in the global sectoral land use fraction map. The List of the datasets used in this 96 method is shown in Table 1. 97 The spatially distributed sectoral GDP map was created in two steps (Figure 1). First, we classified country level GDP data 98 into three sectors: the agriculture, service, and industry sector, and they are downscaled to a spatial resolution of 30 arcsec 99 based on population data, referred as population-based map (PB-method). Second, downscaled estimates are reallocated to 100 the corresponding land use fraction maps derived from satellite products, referred to as land-use-based map (LUB-method). 101 For both the agriculture and service sectors, we generated PB-method and subsequently reallocated them using land-use data. 102 This two-step allocation is necessary because GDP is generally correlated with population distribution (Chen et al., 2022; 103 Kummu et al., 2025), and service-sector GDP, in particular, is strongly influenced by urban agglomeration effects 104 (Morikawa, 2011). However, previous studies have shown that at high spatial resolutions, population data alone may not 105 adequately preserve these correlations (Murakami and Yamagata, 2019; Ru et al., 2023). Therefore, integrating land-use 106 information is essential to ensure spatial consistency. Unlike the agriculture and service sectors, industry sector GDP doesn't 107 necessarily follow population distribution. It often expands into suburban or rural areas with low population density (Zhuang 108 and Ye, 2023). Accordingly, we bypass the PB-method step and directly allocate country-level industrial GDP to land use 109 data. The List of the datasets used in this method is shown in Table 1. 110





113 Figure 1: Flowchart of (top) data processing and (bottom) creation of spatial distributed gross domestic product (GDP) maps of 114 Thailand for the (a) service, (b) industrial, and (c) agricultural sectors.

Data	Format	Datatype	Values range	Spatial resolution	Temporal resolution	Data source, Reference
Built up surface area Non-residential surface	Raster	UInt16	0-10000	100m	five years interval (1975-2020)	Global Human Settlement Layer (Pesaresi and Politis, 2022)
area			0,1		five years interval	
Crop land area	Raster	Boolean	(0 - no croplands, 1 - croplands)	0.9 arcsec	(2003-2019)	Potapov et al., 2022
Population count	Raster	Float64	0-Inf	30arcsec	five years interval (1975-2020)	Global Human Settlement Layer (Pesaresi and Politis, 2022)
Administrative units	Vector (Polygon)	-	-	-	-	GADM 4.1 (2023) Level 1 Layer

116

Data	Format	Datatype	Values range	Spatial resolution	Temporal resolution	Data source, Reference
Built up surface area					five years interval	Global Human Settlement Laver
Non-residential surface area	Raster	UInt16	0-10000	100m	(1975-2020)	(Pesaresi and Politis, 2022)
Crop land area	Raster	Boolean	0,1 (0 - no croplands) 1 - croplands)	0.9 arcsec	five years interval (2003-2019)	Potapov et al., 2022
Population count	Raster	Float64	0-Ir	Parcsec	five years interval (1975-2020)	Global Human Settlement Layer (Pesaresi and Politis, 2022)
City area polygons	Vector (Polygon)	-	-	-	-	Global Rural-Urban Mapping Project v1 (CIESIN, 2011)
Administrative units	Vector (Polygon)	-	-	-		GADM 4.1 (2023) Level 1 Layer

117 Table 1: List of the datasets used in this study.

118 2.1.1 Population-based sectoral GDP

119 In the first step, country-level GDP was partitioned into three sectors and then spatially distributed in proportion to population data at a 120 spatial resolution of 30 arcsec. We used GDP data published by the World Bank (2023), which includes both annual GDP values and their 121 sectoral ratios for the service, industrial, and agricultural sectors, and the Global Human Settlement Layer (GHSL) population grid 122 (R2023; Pesaresi and Politis, 2022) as the source of the global gridded population map. The definition of each sector is shown in Table 2. 123 This downscaling method has been widely employed in previous studies (Kummu et al., 2018; Murakami and Yamagata, 2019) and will be 124 utilized in a later section for comparison with the new method proposed in this study.

126 In the second, step, we reallocated PB-method to global sectoral land use fraction map. In the first step, we used land use 127 elassification maps from satellite products to produce a global sectoral land use fraction map. We generated a sectoral land 128 use fraction map classified into three sectors (service, industry, and agriculture) and three land use type maps with different 129 spatial resolutions: residential (RES), non-residential (NRES), and cropland (CROP). To distinguish RES and NRES areas, 130 we used Global Human Settlement Layer (GHSL) (Pesaresi and Politis, 2022) built-up surface (R2022) data. This layer has 131 100 × 100 m resolution; each pixel has a value of 0-10,000 m2 and residential or non-residential areas may be present within

132 one pixel. For the CROP area, we used the global map of cropland extent (Potapov et al., 2022), provided by Global Land 133 Analysis & Discovery, which has a global spatial resolution of 0.9 arcsec. Maps with the three classes were resampled and 134 combined into a single global sectoral land use (residential, non-residential, and cropland) fraction map at 30 arcsec 135 resolution.

136

137 First, we upscaled the land use maps and simultaneously converted the value of each pixel in both maps into the sectoral 138 fraction within one pixel. In each pixel, RES and NRES had values of 0–10000 m2 and CROP had a value of 0 or 1 (not 139 cropland or cropland). We upscaled the land use maps to 30 arcsec resolution from RES and NRES at a resolution of 100 × 140 100 m and CROP at a resolution of 0.9 arcsec using the GDAL averaging method (GDAL/OGR contributors. 2024). Using 141 the 30 arcsec maps, we calculated the area attributed to each land use type in one pixel with a size of 1 × 1 arcsec and 142 obtained land use fractions for each pixel. Because RES/NRES and CROP had different data sources, the total of the three 143 land use type fractions was greater than one in some pixels. Therefore, we assumed that the CROP fraction could fill only 144 areas that were not designated as RES or NRES. Under this assumption, we modified the CROP fraction in each pixel as 145 follows:

$$146 \ MCROP_{i} = min(CROP_{i}, (1 - RES_{i} - NRES_{i}))$$

$$(1)$$

147 where $MCROP_i$ is the modified CROP fraction in pixel i, $CROP_i$ is the original CROP fraction, RES_i is the RES fraction,

148 and $NRES_i$ is the NRES fraction.

149 After this modification, RES, NRES, and MCROP were considered to represent the service, industrial, and agricultural land 150 use sectors, respectively.

151 2.1.3 Land-use-based agriculture sector GDP

153 beneficiary-supplier relationship. Specifically, agricultural production occurring in peri-urban or rural areas surrounding 154 major population centers is regarded as supplying food and resources to those urban beneficiaries. These agricultural zones, 155 while themselves sparsely populated, are functionally integrated with the urban economy. Therefore, they are expected to 156 exhibit higher GDP values than similarly sparse regions that are not spatially or economically connected to urban demand. 157 To capture this spatial interdependence, the supplier effect applies a distance-decay reallocation from beneficiary pixels in 158 PB-method to nearby supply-side pixels, namely those identified as MCROP. Technically, this is implemented as a linear 159 decay function, in which full weight is given within an inner threshold of 150 km, and weight decrease linearly to zero at an 160 outer threshold of 300km.

161
$$w_{ij} = if d_{ij} \le d_{in}$$
: 1; $if d_{in} < d_{ij} \le d_{out}$: $1 - (d_{ij} - d_{in}) / d_{in}$; $if d_{ij} > d_{out}$: 0 (2)

162 In the second step, we spatially distributed the country-level GDP onto the global sectoral land use fraction map generated in 163 the first step. We used GDP data published by the World Bank (2023), which includes both yearly GDP values and their 164 sectoral ratios for the service, industrial, and agricultural sectors. The definition of each sector is shown in Table 2. For 165 industrial and agricultural GDP, we assumed that the sectoral GDP per area was the same in all the areas of that sector within 166 each country; thus, the industrial and agricultural GDP were distributed only in proportion to the sectoral area fractions of 167 each pixel, with a size of 30 × 30 aresec.

168

Sector	Definition of ISIC		
Agriculture	ISIC 01-03 (A)		
Service*	ISIC 50-99		
Industry	ISIC 05-43 (B-F)		

^{*}Noted that only the Service sector is based on ISIC Rev. 3.

170 Table 2: Definition of each sector, based on the International Standard Industrial Classification (ISIC) Rev 4, in the GDP data 171 by the World Bank (2023).

172 ∰

173 2.1.4 Land-use-based service sector GDP

174 Similarly, PB-method of the service sector is reallocated to residential areas (RES) by applying the supplier effect. The 175 rationale here differs slightly from that for agriculture. Grid-scale population data (e.g., at 30 arcsec resolution, or 176 approximately 1 × 1 km per pixel) are too fine to represent realistic service usage, since people commonly travel more than 177 1 km by car or public transportation to access services (Ciccone and Hall, 1996). Therefore, this reallocation is designed to 178 represent commuting patterns, where service activities in peri-urban zones support nearby urban demand centers. In this 179 context, we use a supplier effect with an inner threshold of 25 km (representing high-intensity interaction) and an outer 180 threshold of 50 km, beyond which service contributions are assumed negligible.

181 2.1.5 Land-use-based industry sector GDP

182 We distributed the industry sector GDP in each country by multiplying the distributed GDP per pixel by the NRES in each 183 pixel. Thus, the distribution was performed for each country, as follows:

184 Industry GDP per pixel_{country} = Total Industry GDP_{country} /
$$\sum_{i=1}^{n} NRES_{i}$$
 (3)

185 $Industry GDP_{country, i} = Industry GDP per pixel_{country} \times NRES_{i}$

(4)¶

186

187 where is the Industry GDP per pixel of sector s in the country, is the total sectoral GDP of industry in the country, is 188 the non-residential area in pixel i, n is the total number of pixels in the country, and is the distributed industry GDP in 189 pixel i in the country.

190 ₩

191 To create a spatially distributed sectoral GDP map, we distributed the sectoral GDP into each sectoral land use area, in each 192 country by multiplying the distributed sectoral GDP per pixel by the sectoral area fraction in each pixel. At this step, we 193 assumed that the distributed sectoral GDP per pixel was the same only within the same country and the same sector. Thus, 194 the distribution was performed for each country and each sector, as follows: ¶

 $\frac{195}{country,s} = \frac{\frac{country,s}{n}}{\sum_{i,s}}$ (2)

 $\frac{196}{country,i,s} = \frac{\times}{country,s} \times i,s \tag{3}$

197 where country,s is the sectoral GDP per pixel of sector s in the country, country,s is the total sectoral GDP of sector s in the

198 country, is the sectoral area fraction of sector s in pixel i, n is the total number of pixels in the country, and country, is

199 the distributed sectoral GDP of sector s in pixel i in the country.

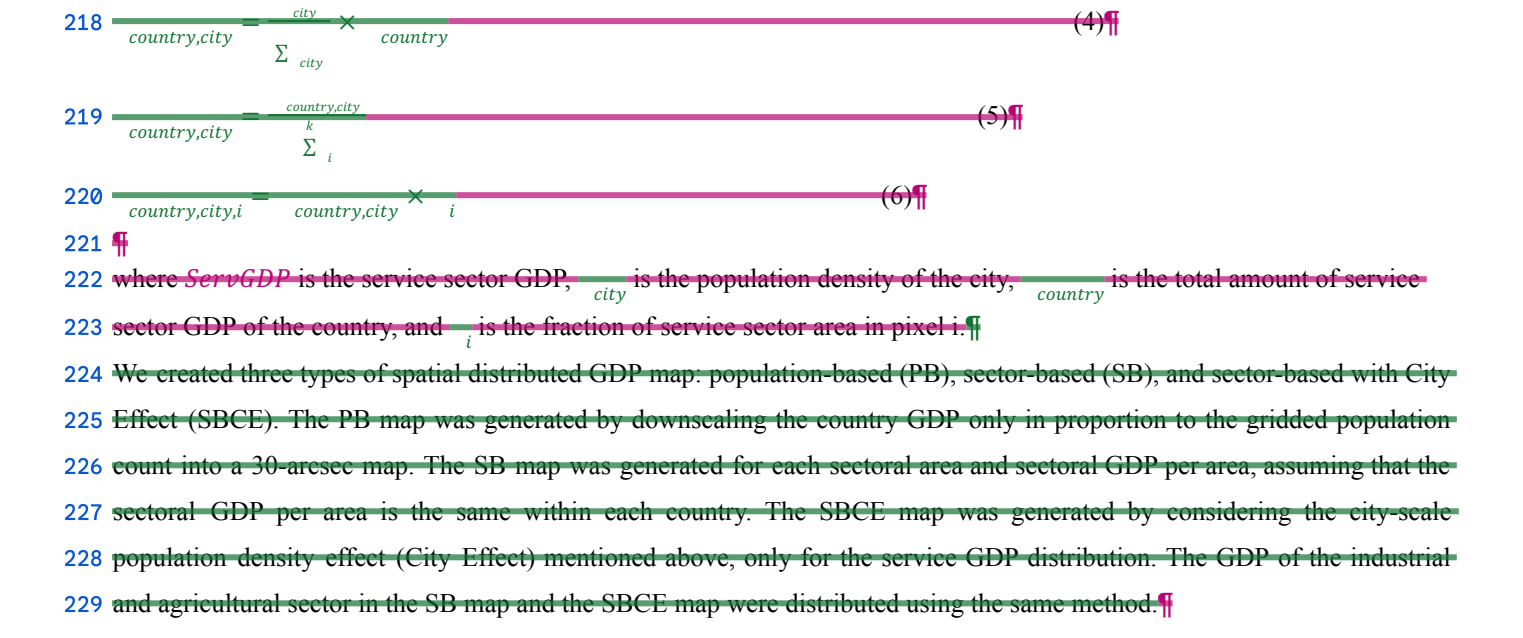
200 ¶

For the service GDP distribution, the activity level in each service sector area depends strongly on the number of people living near that area and using services (Morikawa, 2011). Therefore, we considered the city effect only for the service sector. As an appropriate scale for counting the number of neighbors using the services of a specific area, the grid-scale population (e.g., 30 arcsec resolution, approximately 1 × 1 km per pixel) is too fine to describe a realistic number of users because many people often travel further than 1 km by car or public transportation. Country and district scales are too broad to reflect the intensity of demand of each area accurately (Ciccone and Hall, 1996). Additionally, population density corresponds more strongly to economic activity than to population counts (Ciccone and Hall, 1996; IMF, 2019). Therefore, we considered the city scale population density information for the service sector GDP distribution (City Effect, Fig. 1).

209 ¶

210 The service GDP was distributed only in pixels within cities and the amount of distributed GDP was proportional to the 211 population density of the city where the pixel is located. To detect pixels included in cities, we used the global city polygon 212 dataset provided by Global Rural-Urban Mapping Project (GRUMP) v1 (CIESIN, 2011). To calculate the population density 213 of each city, we used the global gridded population map provided by GHSL population grid (R2023; Pesaresi and Politis,

214 2022). For the distribution of service sector GDP, we first masked out the fractions of the service sector in pixels that did not 215 belong to any city detected using the global city polygon dataset. We distributed GDP into only pixels that belonged to cities, 216 and we assumed that the GDP per area was the same in one city and that the amount of gridded GDP was in proportion to the 217 service sector fraction of each pixel. This calculation was performed as follows:¶



230 2.2 Comparison of GDP distribution methods

231 We created two types of spatial distributed GDP map: population-based (PB-method), Land-use-based (LUB-method). The
232 PB map was generated by downscaling the country GDP only in proportion to the gridded population count into a 30 arcsec
233 map. The LUB-method was generated for each sectoral area and sectoral GDP per area. To assess the effectiveness of the
234 proposed LUB mapping approach, we compared it against PB-method using the DOSE dataset (Wenz et al., 2023), which
235 provides sectoral GDP estimates at the sub-national administrative unit level (GADM level 1). Both GDP maps (i.e.,
236 PB-method and LUB-method) were spatially aggregated from 30 arcsec resolution to the corresponding GADM Level 1
237 administrative boundaries to enable direct comparison with DOSE data. Comparison involved three steps: (1) Scatter plots
238 were generated to evaluate the agreement between the aggregated values from each GDP map and corresponding sectoral
239 GDP values from the DOSE dataset (agriculture, service, and industry) used as reference data. (2) For each method and
240 sector, we computed the absolute value of the relative error between estimated and reference GDP values and derived the
241 cumulative distribution functions to illustrate the distribution of errors across all administrative units. (3) We computed the
242 difference in absolute relative errors between the LUB-method and PB-method to evaluate the improvement or deterioration
243 in accuracy. For each administrative unit, this metric was calculated as:

244
$$\Delta E = E_{LUB} - E_{PB}$$
, where $E = \frac{\left|GDP_{estimate} - GDP_{DOSE}\right|}{GDP_{DOSE}}$ (5)

245 A negative value of (ΔE) indicates that LUB-method is closer to the reference than PB-method (i.e., an improvement), while 246 a positive value indicates a deterioration in accuracy compared to PB-method. The comparison was conducted using only 247 administrative units for which all three sectoral GDP values were available for the year 2010. In total, the comparison 248 included 1,165 administrative units across 57 countries.

250 3 Results

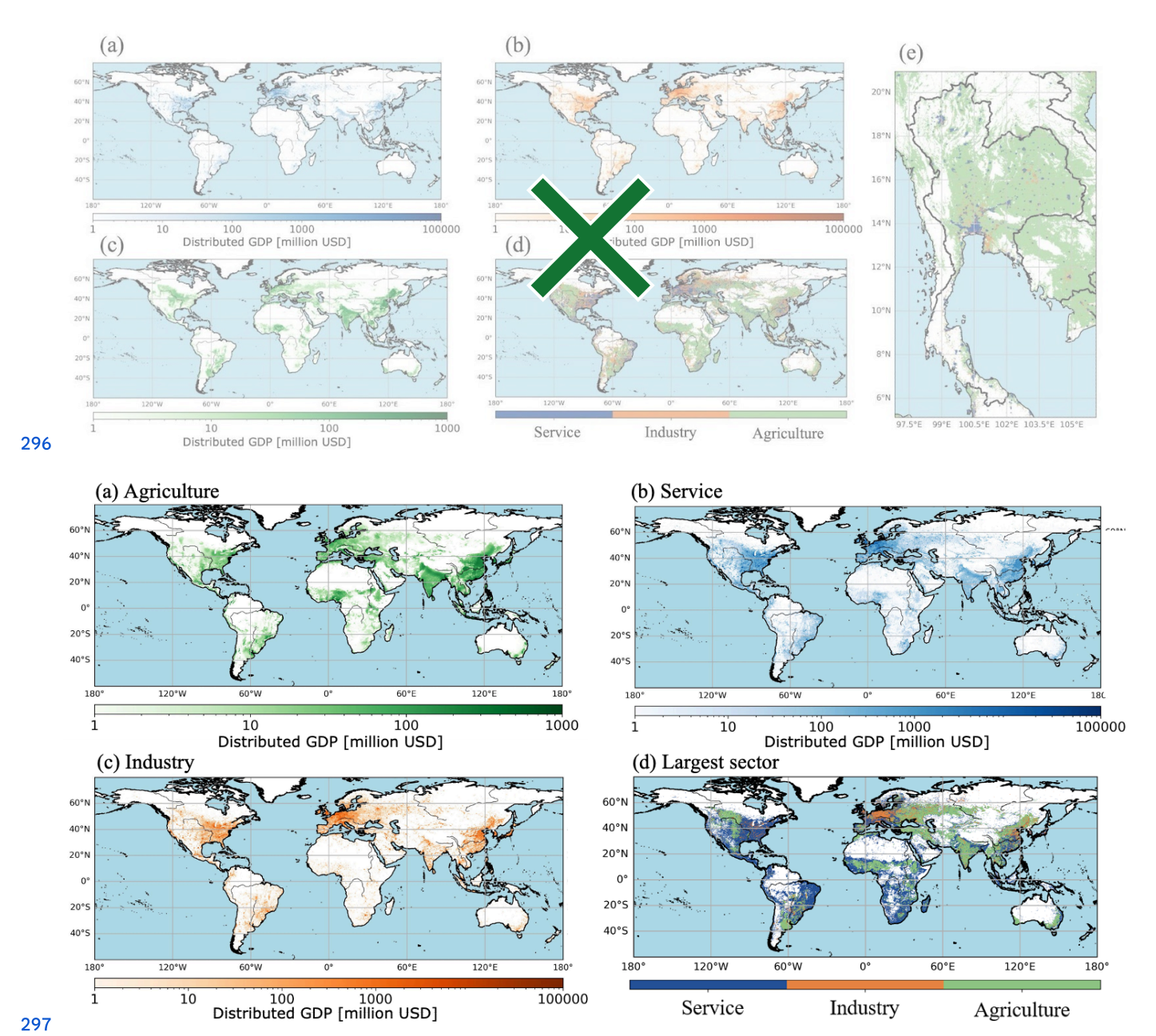
249

We developed three GDP maps for service, industry, and agriculture sectors in 2010, 2015, and 2020. We excluded other 252 years because of the low coverage of national GDP statistics in the World Bank data. Hereafter, the map generated using the 253 LUB method within the Methods will be referred to as "SectGDP30", and the map generated using the PB method will be 254 referred to as "PB-method". The maps of SectGDP30 developed sectoral GDP maps are shown in Fig. 2 (a), (b), and (c). 255 Additionally, to clarify the difference of spatial distribution among sectors, we showed (d) the map of the largest GDP sector 256 in each grid in the world and (e) around Thailand as an example. Globally, the distribution of economic sectors generally 257 correlates with population distribution, with concentrations observed in urban centers. However, variations exist in the 258 detailed distributions. The service sector's distribution predominantly concentrates in urban areas across countries, consistent 259 with population distribution patterns and the use of residential data. In contrast, industrial GDP, proxied by non-residential 260 areas, shows a tendency toward greater concentration in coastal regions. Conversely, agricultural GDP, while exhibiting 261 some correlation with population distribution, is characterized by a more expansive distribution in inland areas compared to 262 the service sector.

263

264 Examining individual countries allows for the identification of more specific differences in the distribution of each sector at 265 a finer scale, shown in Fig. 3. In the figure of Japan, Japan's three major metropolitan areas—Tokyo, Osaka, and 266 Aichi—shows variations in sectoral distribution, despite their common characteristic of high population concentration. In the 267 GDP map, the service sector predominates in the coastal areas of Tokyo and Osaka, which are marked by high population 268 and service industry presence. In contrast, Aichi's coastal regions exhibit a widespread predominance of industrial GDP. 269 Industrial GDP is not uniformly distributed across the entire Aichi area. Within Aichi, the more inland urban center, such as 270 the Nagoya area, shows a prevalence of the service sector, with industrial GDP concentrated in coastal areas. These findings 271 align with Aichi's higher proportion of industrial GDP compared to Tokyo and Osaka (DOSE, 2024), and the formation of an 272 extensive industrial belt along its coastal regions. This dataset facilitates the depiction of detailed distributional differences 273 within these areas.

275 When comparing central Bangkok with its southeastern region, a similar pattern emerges as a case in Japan. The southeastern 276 area, specifically the Eastern Seaboard and Eastern Economic Corridor (EEC) centered around Laem Chabang Port, has 277 developed as an industrial hub. In this region, industrial GDP predominates over service sector GDP. Regarding the 278 distribution of agricultural GDP. Japan shows fewer pixels where agricultural GDP is dominant, largely because much of its 279 agricultural land is located relatively close to urban areas. However, in Thailand and France, extensive areas with dominant 280 agricultural GDP are observed around metropolitan centers like Bangkok and Paris. For instance, Figure 4 (a), which shows 281 only agricultural GDP for France, illustrates that agricultural GDP is minimally developed around densely populated Paris. 282 Conversely, it depicts widespread agricultural activity in the less populated surrounding regions. 283 - Although the GDP maps were produced with a spatial resolution of 30 arcsec, these maps in Fig. 2 show the aggregated 284 maps into 0.5 degree. These GDP maps are those called GDP-LULC SBCE in the Methods. Both maps of the service and 285 industry sector showed the same shape of extents which have each sector GDP. Meanwhile, the GDP accumulation into the 286 center of the economic activity was different between them. Looking at the east part of the United States, while industry 287 GDP was scattered evenly in a wide area, service GDP accumulated intensely in some centers of cities and other areas have 288 much smaller GDP in those places. This tendency was not the ease with other countries. In countries such as India and Iran, 289 the industry GDP was more concentrated in some specific areas than the service GDP. As for the agriculture GDP, compared 290 to maps of those two sectors, the GDP was spread to a much wider area with less concentration in specific areas. Even with 291 this different characteristic, the agriculture GDP was basically distributed aligning with the other two sectors' GDP. When 292 we look at the map around Thailand (Fig. 2 (e)), we can see the different distribution between each sector. While the service-293 GDP (blue) dominated in the Bangkok area, the industry GDP mainly dominated in the eastern area, next to the Bangkok 294 area. The sectoral GDP map of this study showed such heterogeneity of each sector on a local scale within one country.



298 Figure 2: The sectoral GDP maps of (a) service sector, (b) industry sector, (c) agricultural sector, (d) the map of the largest GDP sector in each grid of 30 arcsec 0.5 x 0.5 degree, and (e) the same map around Thailand.

300 We validated this different distribution of each sector's GDP using subnational sectoral GDP statistics of Thailand in 2009 301 provided by the Thailand government (NESDC, 2016) as reference data. We spatially aggregated the GDP map into seven 302 districts corresponding to the statistics classification: Northeastern, Northern, Southern, Eastern, Western, Central, and 303 Bangkok & Vicinity (Fig. 3). This aggregation was performed using the administrative area polygon dataset obtained by

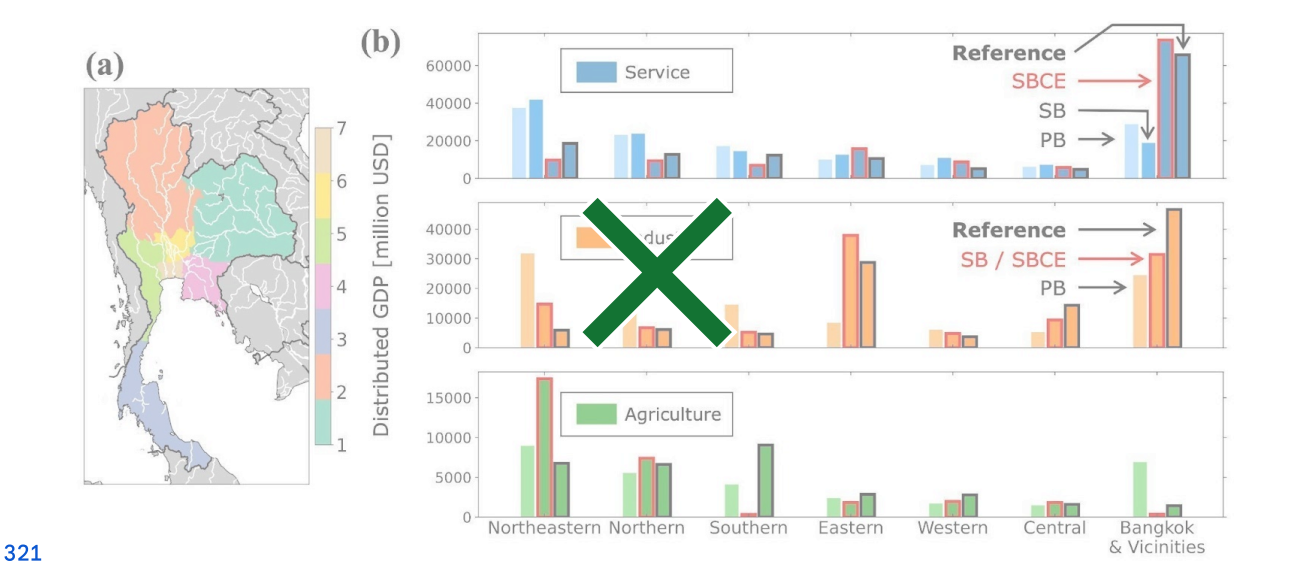
GADM 4.1 (2023) and its correspondence with the district definition in the statistics. The spatially aggregated GDP of each sector in each district of the three maps (PB, SB, SBCE) and the Thailand government statistical values (Reference) are shown in Fig. 3. The population based map had no information on sectoral differences among districts; therefore, the sectoral ratio of the gridded GDP value was assumed to match that of the entire country in all pixels and districts, following the practice of previous studies (Willner et al., 2018; Tanoue et al., 2020). As an index of consistency of the three maps with Reference, we calculated average relative errors (ARE) of the aggregated district GDP in each map to Reference, on an average of all seven districts, as follows:

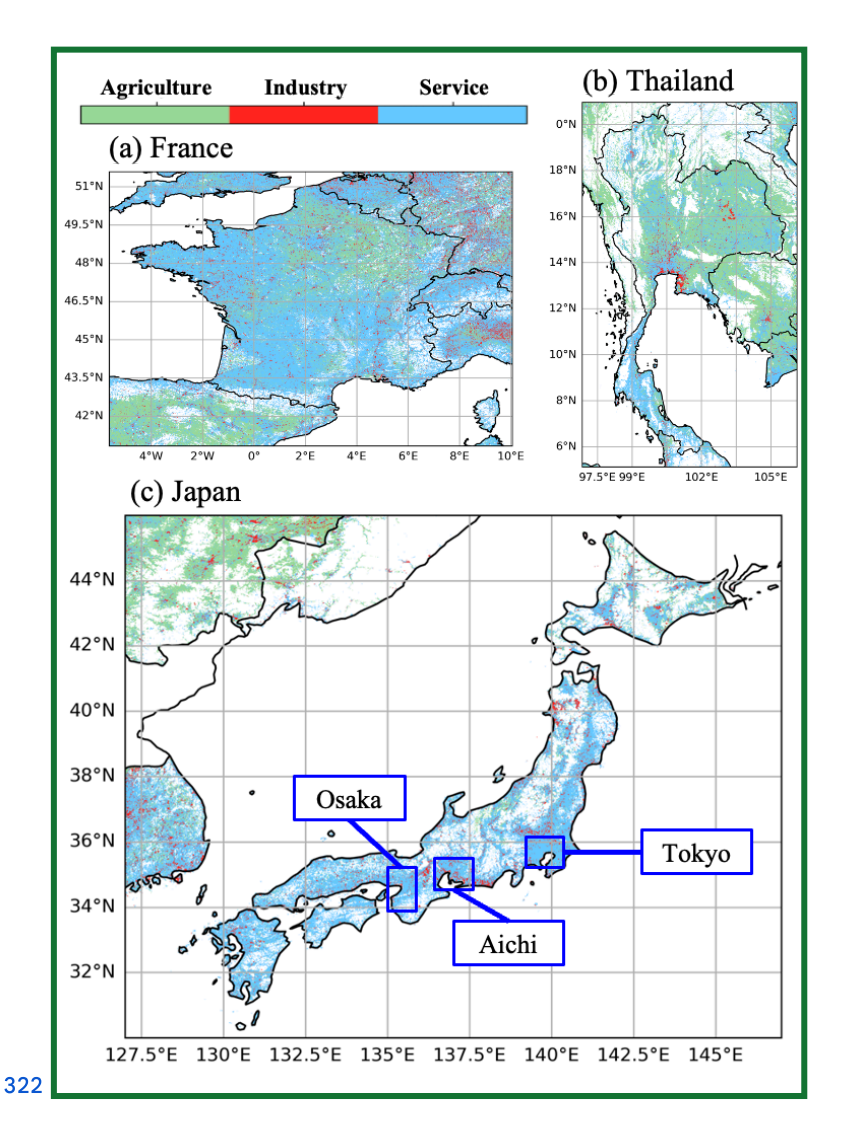
$$311 \ ARE[\%] = \frac{7}{7} \sum_{k} \left| \frac{k \ k}{k} \right| \times 100 \tag{7}$$

312 where k is the number of each district shown in Fig. 3.¶

320

313 The AREs for the total GDP values of the PB, SB, and SBCE maps were 63.0%, 50.0%, and 26.2%, respectively. These 314 AREs consisted of errors of each sector in each district. For the service sector, the AREs were 50.3%, 69.2%, and 38.6%, 315 respectively, in the PB, SB, and SBCE map. The largest service GDP was seen in Bangkok & Vicinity in Reference. While it 316 was seen in the same district in the SBCE map, the different district (Southeastern) had the largest in the other two maps (PB 317 and SB). This result meant the SBCE showed better consistency with Reference than PB and even SB. This indicated that 318 solely using the residential fraction map was not enough to express the spatial distribution of service GDP and the city-scale 319 population density could help to reproduce the actual GDP distribution.





332

323 Figure 3:-(a) The seven districts of Thailand (1, Northeastern; 2, Northern; 3, Southern; 4, Eastern; 5, Western; 6, Central; 7, 324 Bangkok and Vicinities). (b) Distributed sectoral GDP of subnational even districts in Thailand in 2009, obtained from the 325 population-based (PB), sectoral-based with city effect (SBCE) maps and statistical values from the government of Thailand 326 (Reference). The map of the largest GDP sector in each grid of 30 arcsec in (a) France, (b) Thailand, and (c) Japan.

328 To validate the accuracy of this GDP map, we conducted a comparative analysis with DOSE, a dataset providing sectoral GDP figures at 329 the sub-national administrative unit level. For this validation, the 30 arcsec resolution GDP map was spatially aggregated according to the 330 GADM dataset's Level 1 administrative divisions, which are used by DOSE. The aggregated GDP values for each administrative unit were 331 then calculated and compared with DOSE's figures.

333 The results are presented in Figure 4 (a), (b), and (c). These three scatter plots indicate that SectGDP30 exhibits a similar distribution to 334 actual sub-national scale sectoral GDP (R^2 > 0.9 in all the sectors). When examined by sector, many administrative units with 335 discrepancies in service and industrial GDP show an underestimation compared to actual data. Given that the total GDP per sector at the 336 national level aligns with real data in this study, this discrepancy likely results from over-distributing GDP in a few administrative units 337 within certain countries, leading to an underestimation in many other smaller administrative units. While service and industrial GDP 338 inherently concentrate in specific local areas, and this GDP map depicts that, some countries show an excessive concentration in particular 339 regions. This trend is less apparent in agricultural GDP, which exhibits less localized distribution, and no strong pattern of 340 overestimation or underestimation was observed.

341

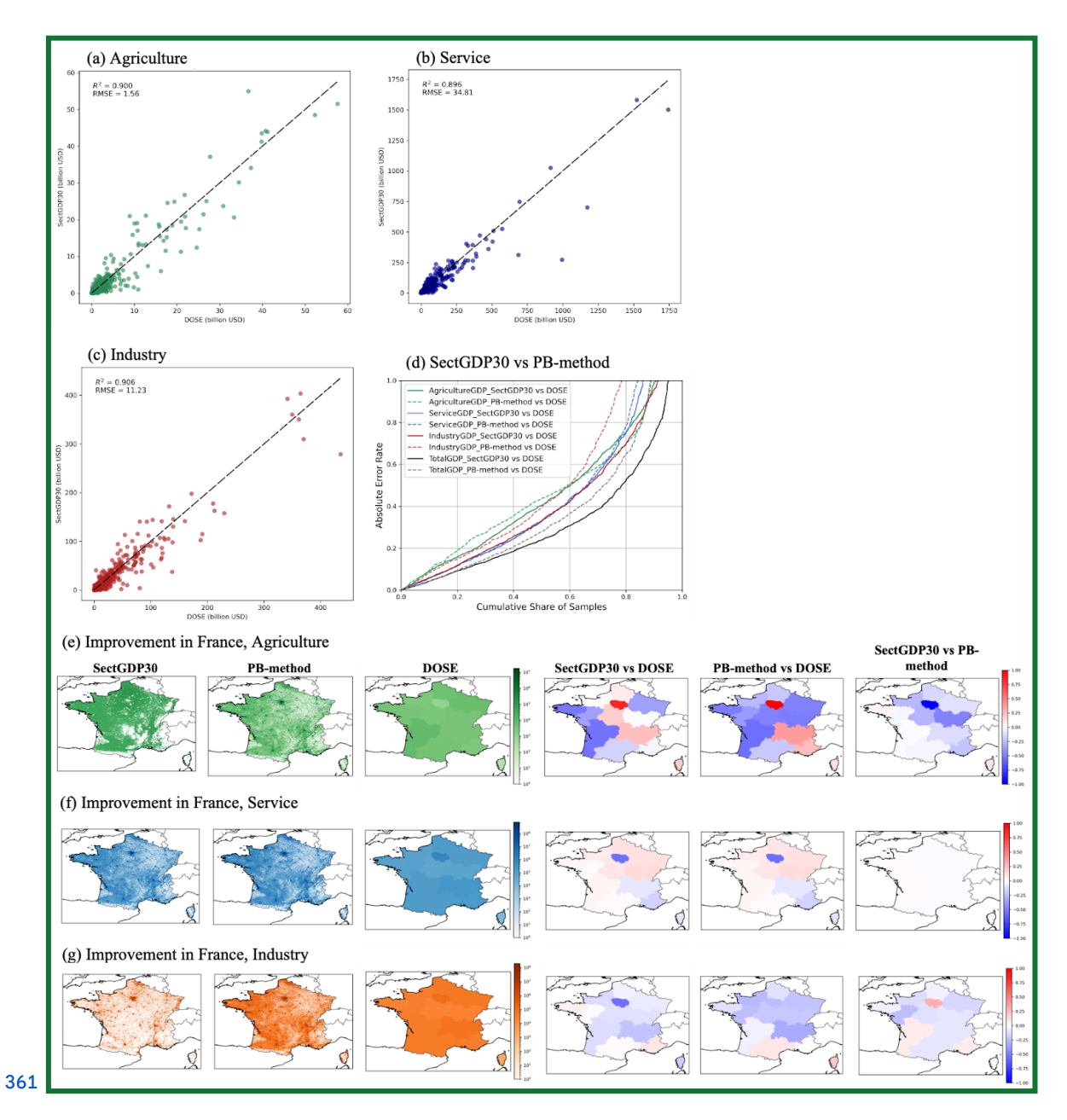
342 Next, we compared the results from SectGDP30 with PB-method. The comparison method involved using sectoral GDP figures for each administrative unit, as before, and calculating the cumulative distribution of the differences from DOSE's figures. This result is presented in Figure 4 (d). Sectoral analysis reveals that the industrial sector shows the most significant improvement when compared to PB-method. As previously mentioned, industrial GDP distribution often exhibits localized concentrations even in sparsely populated areas. This suggests that a method using only non-residential land use information and concentrating distribution over relatively small areas is more appropriate than PB-method, which relies on population distribution data.

348 The service sector shows a slight decline in accuracy compared to PB-method. In the service sector, overall regional results showed a 349 slight decrease in accuracy for SectGDP30 compared to PB-method. However, some regions exhibited improved accuracy with 350 SectGDP30. Fundamentally, there is minimal difference between SectGDP30 and PB-method as the spatial distributions of residential 351 areas (upon which SectGDP30 relies) and population (upon which PB-method relies) largely coincide.

352 Conversely, SectGDP30 incorporates Supplier effect, reallocating each grid's GDP to residential areas within a 50km radius. This results in a smoother connection of urban and rural area distribution differences compared to PB-method. This effect is evident in the Alpine regions of Switzerland (CHE), specifically in administrative level districts such as Uri, Wallis, Graubunden, and Glarus. While these Swiss Alpine areas have a significant population, residential areas are limited, and actual statistical service GDP is not high. Therefore, in Switzerland, service GDP should be distributed not based on simple population distribution but rather in the plains north of the Alps, where numerous residential areas exist. This case demonstrated an improvement in SectGDP30 accuracy. Agricultural GDP also shows an improvement service of the PB-method, with an increase in the number of administrative units exhibiting smaller errors.

359

360



362 Figure 4: The scatter graphs of the municipality GDP for (a) service sector (b) industry sector (c) agriculture sector and (d) the 363 cumulative distribution of the errors between DOSE and SectGDP30 and between DOSE and PB-method for each sector.

365 For the industrial sector, the AREs were 159% and 42.7% in the PB and SB/SBCE map, showing the PB map had a marked 366 inconsistency to Reference. On the other hand, SB/SBCE maps could express the large industry GDP in districts such as

367 Eastern and Central. This indicated that the accumulation of non-residential fraction, which was hypothetically assumed to 368 correspond to industry GDP in this study, corresponded well with the distribution of industry sector activities.¶
369 ¶

370 Conversely, for the agriculture sector, which was spatially distributed using the same method as for the industrial sector, 371 none of the three maps could show the largest agriculture GDP in the Southern district. The SB/SBCE map showed an 372 overestimation in Northeastern and underestimation in Southern and Bangkok & Vicinity. This indicated that the cropland 373 fraction map used in the Method could not express the intense accumulation of agriculture GDP. The cropland map used in 374 this study has no information on crop types; thus, the productivity of individual crop types was ignored for each district in 375 Thailand. For example, the Northeastern district produces mainly rice with low land productivity, whereas the Southern 376 district produces natural rubber and palm oil (Inoue, 2010). This heterogeneity of "production in monetary unit per area" was 377 not considered in this study, which probably led to the low improvement of GDP distribution accuracy in the SB/SBCE map.

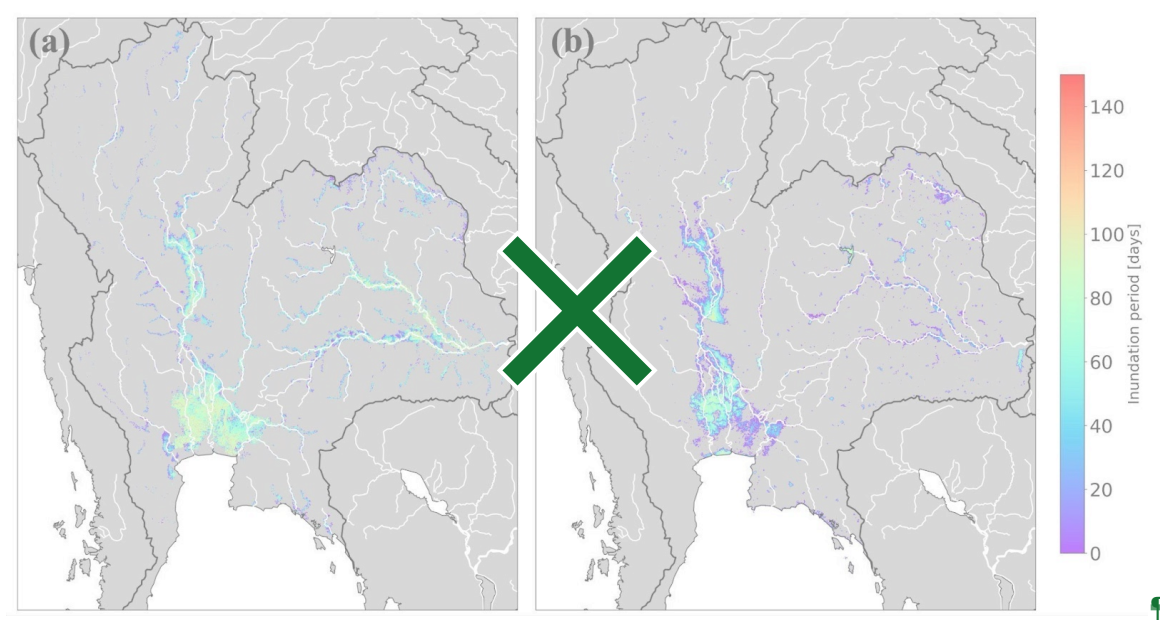
378 4 Discussion - Business interruption loss estimation for the 2011 Thailand flood 4.1 Business interruption loss 379 estimation for the 2011 Thailand flood

380 To assess how the improvement of the GDP map affects the result of flood loss estimation, an additional analysis of 381 estimating business interruption losses resulting from the actual flood event in Thailand in 2011 by the new sectoral GDP 382 map was conducted. Following established definitions of economic losses from prior studies (Tanoue et al., 2020; Rose, 383 2004), economic impacts can be categorized into three main types: damage, direct economic loss, and indirect economic 384 loss. This additional analysis focused exclusively on estimating Business Interruption loss (BI loss) among these three 385 economic impacts due to the lack of information necessary for the estimation of the other components.

386

387 To calculate BI loss, we prepared hazard, exposure, and vulnerability data. As the hazard, we used two inundation period 388 maps of the target event in Thailand, based on simulation and satellite observations. The simulation-based inundation period 389 map was generated using the Catchment-based Macro-scale Floodplain (CaMa-Flood) global riverine inundation model 390 (Yamazaki et al., 2011). To obtain an inundation map based on the simulation by CaMa-Flood, CaMa-Flood used daily 391 runoff data generated by a reduced-bias meteorological forcing dataset at 15-arcmin resolution, and S14FD-Reanalysis data 392 (Iizumi et al., 2017) to simulate the daily inundation depth at 15-min resolution. Because S14FD is a bias-corrected dataset, 393 we used daily inundation depth values without bias correction, such that the inundation period may be calculated directly 394 from the daily inundation depth (Taguchi et al., 2022). Then, we downscaled the 15-arcmin daily inundation depth to 30 395 arcsec resolution and calculated the inundation period as the number of days in which the inundation depth exceeded 0.5 m 396 in each pixel. We also used an inundation period map based on Terra/Moderate Resolution Imaging Spectroradiometer 397 (MODIS) images, which is publicly available on the Global Flood Database (Tellman et al., 2021). We referred to the former

398 hazard map as "CaMa-Flood" and the latter map as "MODIS" in this study. The days between August and December in 2011 399 were only counted as inundation days for matching the inundation period by CaMa-Flood simulation and that by MODIS 400 observation, which started from August and ended around the end of December. The inundation period maps of CaMa-Flood 401 and MODIS are shown in Fig. 4.



402

403

406

404 Figure 4: Spatial distribution of the inundation period of the 2011 Thailand flood, obtained from (a) Catchment-based Macro-scale 405 Floodplain (CaMa-Flood) simulation and (b) Moderate Resolution Imaging Spectroradiometer (MODIS) observation data.

407 As exposure, we used two spatial distributed GDP maps at 30 arcsec resolution for comparison, SectGDP30 and 408 PB-methodthe population-based map (PB) and the sector-based map with CE (SBCE). As a vulnerability, we considered a 409 recovery coefficient, which decided the ratio of the length of recovery period which is required until business restart to the 410 inundation period. This value reflects the system vulnerability of the city. We used 2 as a recovery coefficient, which was 411 used in previous study on a global scale (Taguchi et al., 2022). As for the recovery period as vulnerability, we used the 412 method of Tanoue et al. (2020). The recovery period RP_i , when the production in a pixel is assumed to have recovered 413 linearly from zero at the end of the flood period to the same level of production before the flood, was obtained by 414 multiplying the inundation period by a coefficient (= 2 in this study). Thus, the recovery period was assumed to take twice as 415 long as the inundation period. Finally, BI loss was estimated by the method described by Tanoue et al. (2020), as follows:

416 BI loss =
$$\sum_{i=1}^{N} \sum_{s}^{3} \left\{ (IP_{i} + \frac{RP_{i}}{2}) \times \frac{AGDP_{i,s}}{Nd} \right\}$$
 (6)

417 where i, N, and s are the pixel number, total number of pixels in the inundated area, and sector number (1 = service, 2 = 418 industry, and 3 = agriculture), respectively; IP_{i} , RP_{i} , $AGDP_{i}$, S, and Nd are the inundation period, recovery period at pixel i,

419 annual GDP of pixel i and sector s, and the number of days in a year.

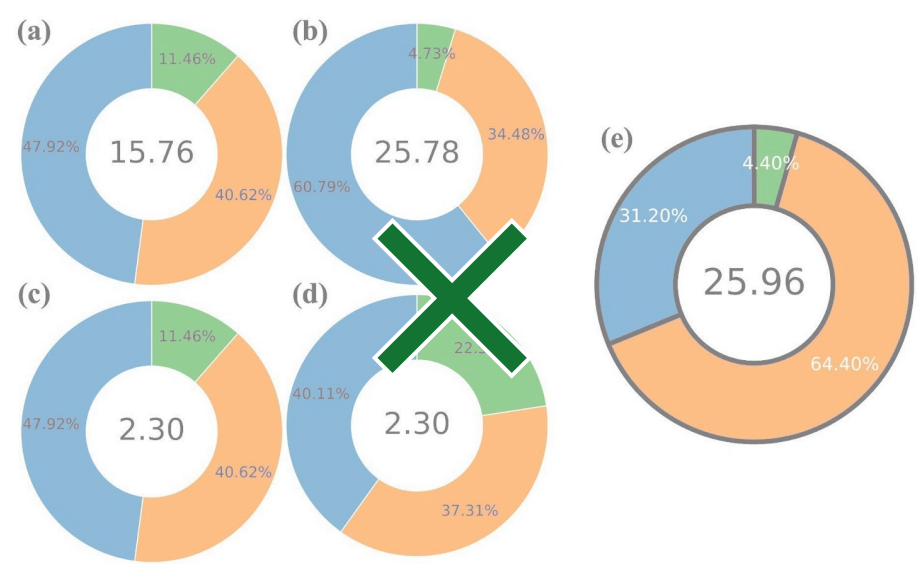
420 And we obtained the total BI losses by summing BI losses of all the grids in the target area.

421

422 The results of the BI loss estimation were shown in Fig. 5. We compared the calculated BI losses with the actual economic 423 loss reported in the PDNA (The World Bank, 2011). In this report, both damage and loss were estimated. Damage is due to 424 the destruction of physical assets and loss is caused by foregone production and income and higher expenditures in the 425 definition in the report. This means that the loss in the report included both business interruption loss and other additional 426 expenditures and costs. Because there was not any other reported loss which only focused on BI loss, we compared with the 427 loss, including other components, in this report.

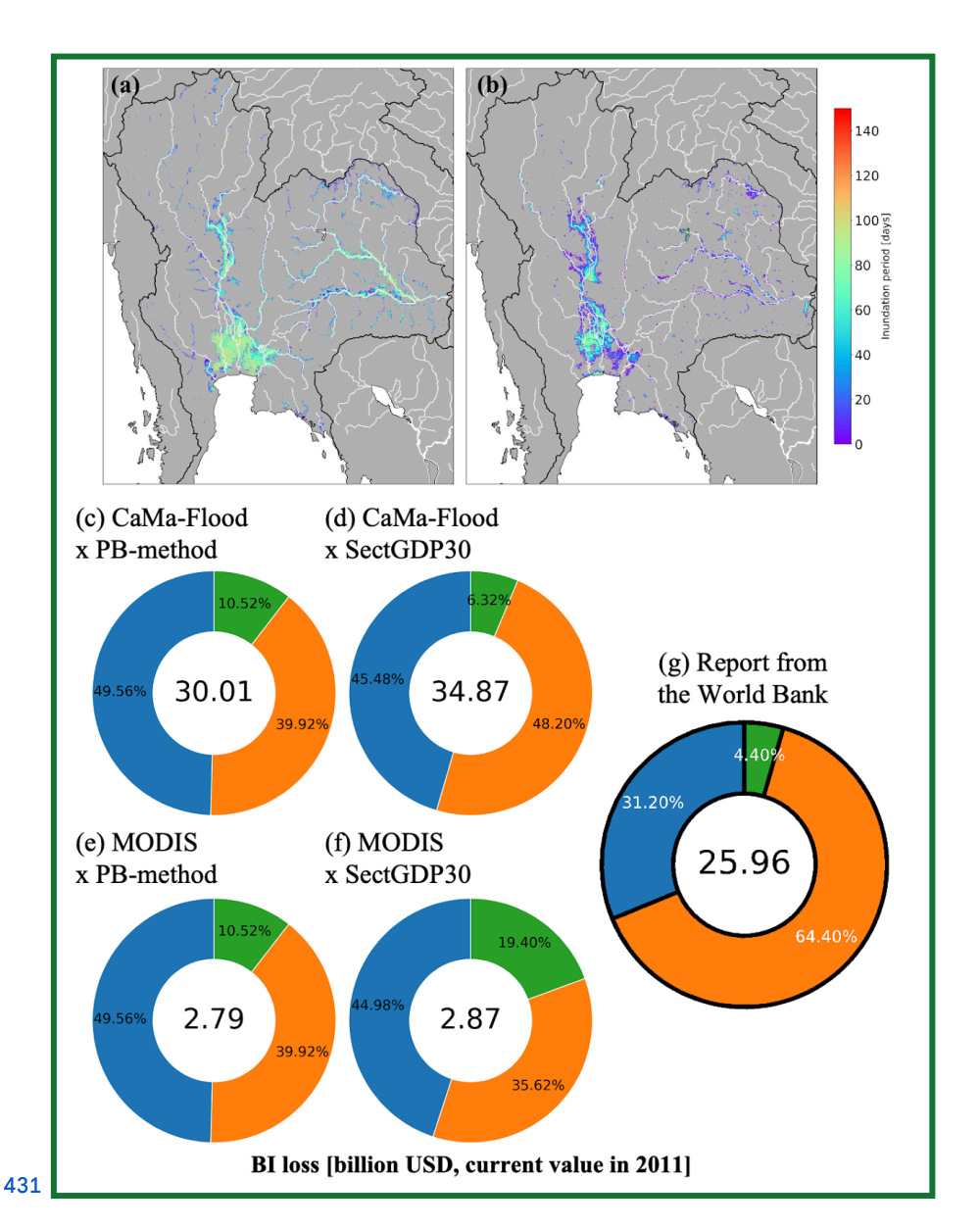
428

429



430

BI loss [billion USD, current value in 2011]



432 Figure 5: Spatial distribution of the inundation period of the 2011 Thailand flood, obtained from (a) 433 Catchment-based Macro-scale Floodplain (CaMa-Flood) simulation and (b) Moderate Resolution Imaging 434 Spectroradiometer (MODIS) observation data, and the simulation Business interruption losses (USD billion, current 435 value in 2011) due to the 2011 Thailand flood, estimated by combining hazards and exposures; the total loss is written 436 in the center of each circle. (c) CaMa-Flood and PB-method, (d) CaMa-Flood and SectGDP30, (e) MODIS and 437 PB-method, (f) MODIS and SectGDP30, and (g) the World Bank report (2011).

439 Firstly, comparing the losses by the different hazard data with the same exposure, SectGDP30 the SBCE map, the service 440 sector loss according to CaMa-Flood (USD 15.8615.67 billion) was over 125-fold larger than that according to MODIS 441 (USD 1.290.92 billion). This large difference was caused by the shorter average inundation period and smaller flood area in 442 MODIS than in CaMa-Flood. MODIS is known to tend to fail to capture the flood extent in urban areas with high densities 443 of tall buildings and that leads to the underestimation in inundation. In addition to different total losses, ratios of 444 industryservice—sector loss to the total loss differed between two results: 48.2060.79% according to CaMa-Flood and 445 35.6240.11% according to MODIS. This result showed the sectoral ratio of the loss can be changed depending on spatially 446 different hazards. It is caused by the fact that SecGDP30 can show the different spatial distribution of each sectoral GDP, 447 while municipality-level statistics cannot show the spatial distribution in a fine resolution. This sectoral difference was newly 448 found by this study since the traditional population-based GDP map also could not show this difference between sectors.

449

450 The result by the set of the hazard of CaMa-Flood and exposure of the LULCSBCE map (b in Fig. 5) was consistent with the 451 reported total loss, although the sectoral losses differed from the report. The total loss differed from the report by only 452 -0.72% (USD 25.78 billion estimated loss vs. USD 25.96 billion reported loss), the service sector loss was overestimated 453 (USD +7.57 billion loss, +29.59 point sectoral loss ratio), and the industrial sector loss was underestimated (USD -7.83 454 billion loss, 29.92 point sectoral loss ratio). In the service sector, the results were overestimated for the larger inundation 455 extent and longer inundation period due to the lack of flood protective effect data in urban areas, where many services are 456 located. Comparing the results using CaMa-Flood and SectGDP30 with the World Bank Report figures (Figure 5 (d) and 457 (g)), SectGDP30 more accurately represents the smaller proportions of agricultural damage compared to when PB-method is 458 used (Figure 5 (c)). This indicates that SectGDP30 can effectively constrain the allocation of agricultural GDP in areas with 459 high population but limited agricultural land. Conversely, while the Report figures show a significant proportion for the 460 industry sector, SectGDP30 results estimate the industry sector to be almost on par with the service sector. It showed the 461 industry loss was underestimated In the industrial sector, although the hazard in the numerical simulation, by CaMa-Flood, 462 captured the flood extent over the industrial sector area and the long-lasting inundation period, the loss was underestimated. 463 The reported value excludes assets damage but includes economic losses other than production reduction by direct contact 464 with the flood, such as production stoppage due to shortages of raw materials induced by blocked roads. Therefore, if we 465 assume that the new sectoral GDP map captured the industrial locations and they were successfully considered to be flooded, 466 this underestimation is presumed to be caused by a lack of data reflecting the indirect production stoppage.

467

468 Related to this limitation of the indirect production stoppage, it is important to recognize that the methodology, including that 469 of this paper and previous studies, which determines the GDP produced in each pixel using indicators such as GDP per unit 470 area, overlooks the fact that labor supplied from remote locations is necessary for GDP production. To rephrase this with the 471 example of a factory affected by a disaster: while the GDP output itself occurs at the factory's location, the workers who

472 carry out the production reside in surrounding or remote areas. Therefore, if a disaster occurs in these remote residential 473 areas, the GDP output should cease. However, pixel-based calculation methods would fail to represent this cessation of GDP 474 output as long as the factory's pixel is unaffected. This is considered a non-negligible impact in regions where economic 475 activity and residential areas are clearly separated, but quantifying this impact on a global scale is currently challenging. 476 Alongside future research on regional differences in GDP per unit area, this remains a limitation that we must consider 477 moving forward.

478 **¶**

In addition to the notable omissions of urban flood protection and indirect production stoppage from the analysis, addressing the inherent uncertainty associated with the recovery coefficient is of utmost importance. This coefficient plays a pivotal role in calculating the recovery period following an inundation event and consequently has a substantial impact on the estimation of business interruption losses, as demonstrated in the equation. However, determining the most appropriate coefficient plays a proves to be a formidable challenge, given its variability across different locations and sectors, a fact substantiated by both Taguchi et al. (2022) and Kimura et al. (2007). Presently, attempting to ascertain the ideal coefficient for each sector is difficult due to the absence of comprehensive observed data. It is crucial that future research investigates this matter.

486 4.2 Limitation¶

487 Firstly, there are uncertainties in the assumption of distributing sectoral GDP in proportion to the fraction of each land use. In 488 the Methods, we decided to consider the other components affecting the spatial accumulation such as population density only 489 in service GDP and assumed GDP per area is uniform in industry and agriculture. However, GDP per area could be different 490 depending on areas. For agriculture, it was indicated that GDP per area depends on the type of crops in the Result. Also, for 491 industry, produce per area was reported as different depending on sub sectors among industry. For example, in Japan, 492 production per area of the chemical products sector is almost five times larger than that of transport equipment (METI, 493 2007). These indications are difficult to utilize for the method of generating the global map because the data related to spatial 494 distribution of crop type and subsectors are not available, which is the different case from the service GDP map using 495 globally available population map. In this study, we indicated the importance of considering other components affecting 496 GDP per area by showing the improvement of service GDP map by City Effect and the low accuracy of agriculture GDP 497 map. Therefore, we expected further research on finding relationships between sectoral GDP per area and indices which 498 could be obtained by public and globally available data such as those provided by satellite observation or public statistics. 499 ¶ 500 Furthermore, it is important to recognize that the methodology, including that of this paper and previous studies, which 501 determines the GDP produced in each pixel using indicators such as GDP per unit area, overlooks the fact that labor supplied 502 from remote locations is necessary for GDP production. To rephrase this with the example of a factory affected by a disaster-503 while the GDP output itself occurs at the factory's location, the workers who carry out the production reside in surrounding

or remote areas. Therefore, if a disaster occurs in these remote residential areas, the GDP output should cease. However, pixel-based calculation methods would fail to represent this cessation of GDP output as long as the factory's pixel is unaffected. This is considered a non-negligible impact in regions where economic activity and residential areas are clearly separated, but quantifying this impact on a global scale is currently challenging. Alongside future research on regional differences in GDP per unit area, this remains a limitation that we must consider moving forward.

509

This study was limited in that the validation and comparison of the GDP map was performed only for Thailand and for the map in 2010. The study methodology should be validated for other countries prior to global applications. However, this is the first study to quantify the differences between traditionally used GDP maps and actual economic activity, and to evaluate how such GDP maps may be improved using satellite products, for countries with large differences in sectoral GDP among subnational districts, such as Thailand. In this point, this study could contribute to the improvement of global natural hazard risk assessment, as the methodology and dataset used in this study can be easily applied to global. For that this study investigated only the map in 2010, although we did not carry out the analysis on the temporal change of sectoral GDP map, the data of land use map and national sectoral GDP we used in this study are available in other multiple years. Thus, the method in this study is applicable also to the analysis on different time series and we expected further analysis on it in the future.

520 5 Data availability

- 521 The global sectoral GDP maps are publicly available via Zenodo at https://doi.org/10.5281/zenodo.13991673 (Shoji et al.,
- 522 2024). The maps on Zenodo correspond to the SBCE maps in this paper and are stored as geotiff files. In total, there are nine
- 523 maps in the dataset, for each sector (service, industry, and agriculture) and year (2010, 2015, and 2020).

524 6 Summary

- 525 This study developed a spatially distributed sectoral GDP map (SectGDP30) by leveraging recently available global,
- 526 high-resolution land use datasets. This map demonstrates strong consistency ($R^2 > 0.9$) with actual sub-national statistical
- 527 data and exhibits greater alignment with sub-national GDP statistics compared to conventional GDP maps (PB-method) that
- **528** rely solely on gridded population maps.

529

- 530 For the industry sector, the methodology successfully distributed industrial GDP with better accuracy than population
- 531 distribution alone. This was achieved by adopting "Non-residential areas" as a proxy, which effectively captures the localized
- 532 nature of industrial GDP distribution in specific regions within each country. For agriculture, accuracy was improved over

PB-method by distributing GDP based on farmland maps and assuming GDP generation in areas approximately 150-300 km from wide-area population centers. Regarding the service sector, incorporating population distribution within specific ranges, even when using residential land use map information, resulted in GDP being distributed only to actual built-up and designated residential areas. This approach achieved an accuracy comparable to PB-method.

537

538 As an application of this dataset, business interruption (BI) loss estimation due to floods was conducted using the sectoral 539 GDP map. This confirmed that the new sectoral GDP map can represent inter-sectoral differences in estimated BI losses, 540 corresponding to varying spatial distributions of hazards. This validation underscores the importance of considering the 541 spatially distinct distributions of sectors when estimating actual disaster damage. It also highlights the need for developing 542 new estimation methods that account for the processes of GDP generation.

543

544 This new global sectoral GDP map serves as a foundational tool for estimating sector-classified economic losses. It 545 meticulously considers the complexity of global land use patterns at a detailed level, enabling accurate calculation of 546 sector-specific losses from various natural disasters on a global scale.

In this study, we generated a spatially distributed sectoral GDP map by leveraging a recently available global detailed land use dataset; the map showed better consistency with subnational GDP statistics than the traditional GDP map did, relying only on the gridded population map. We found that the land use classification of residential and non-residential areas could be used to spatially distinguish the service and industrial sector areas. The accumulation of non-residential areas worked well—as a proxy of industrial sector production intensity. Conversely, that of residential areas was insufficient to express the high accumulation of economic activity by the service sector in large cities. To overcome this problem, we considered the accumulation in the service GDP distribution and is a globally available satellite product. For the agricultural sector, we determined that it is necessary to incorporate crop type information.

556 ₩

The flood BI loss estimation using the sector-based GDP map confirmed that the new sectoral GDP map was able to express sectoral differences in the estimated BI loss, depending on the different spatial distributions of hazard. The underestimation of the industrial sector loss was probably resulting from a lack of data reflecting the effect of transportation network disruption. To consider the loss due to such transportation disruption and estimate more realistic economic losses, it is necessary to include information on both the road network and transportation of goods for the industrial sector by combining road network data and transportation statistics between each area within each country.

563 ₩

- 564 This new sectoral GDP map in global can serve as a foundation for estimating economic losses classified by sector while-
- 565 meticulously accounting globally for the intricacies of land use patterns. This enables precise calculations of sector-specific
- 566 losses by various natural hazards on a global scale.

568 Competing interests

569 The contact author has declared that none of the authors has any competing interests.

570

571 Acknowledgement

- 572 This work was supported by Japan Science and Technology Agency (JST) [Moonshot R&D; JPMJMS2281] and Ministry of
- 573 the Environment of Japan / Environmental Restoration and Conservation Agency [Development Fund;
- **574** JPMEERF23S21130].

575

576 References

- 577 Alfieri L, Bisselink B, Dottori F, Naumann G, De Roo A, Salamon P, Wyser K, Feyen L.: Global projections of river flood
- **578** risk in a warmer world. Earth's Future 5: 171-182, 2017.
- 579 Bontemps S, Herold M, Kooistra L, Van Groenestijn A, Hartley A, Arino O, Moreau I, Defourny P.: Revisiting land cover
- 580 observations to address the needs of the climate modelling community. Earth System Science/Response to Global Change:
- 581 Climate Change, Preprint Report, 2011.
- 582 Chen, J., Gao, M., Cheng, S., Hou, W., Song, M., Liu, X., & Liu, Y.: Global 1 km× 1 km gridded revised real gross domestic
- 583 product and electricity consumption during 1992–2019 based on calibrated nighttime light data. Scientific Data, 9(1), 202,
- **584** 2022.
- 585 Ciccone A, Hall RE.: Productivity and the density of economic activity. The American Economic Review 86: 54-70.
- 586 http://www.jstor.org/stable/2118255, 1996.
- 587 CIESIN (Center for International Earth Science Information Network).: Global Rural-Urban Mapping Project, Version 1
- 588 (GRUMPv1): Urban Extent Polygons, v1.02, 2011.
- 589 De Moel H, Van Vliet M, Aerts JCJH.: Evaluating the effect of flood damage-reducing measures: a case study of the
- 590 unembanked area of Rotterdam, the Netherlands. Regional Environmental Change 14: 895–908, 2014.

- 591 Dottori F, Szewczyk W, Ciscar J, Zhao F, Alfieri L, Hirabayashi Y, Bianchi A, Mongelli I, Frieler K, Betts RA, Feyen L.:
- 592 Increased human and economic losses from river flooding with anthropogenic warming. Nature Climate Change 8: 781-786,
- **593** 2018.
- 594 Duan Y, Xiong J, Cheng W, Li Y, Wang N, Shen G, Yang J.: Increasing Global Flood Risk in 2005–2020 from a Multi-Scale
- 595 Perspective. Remote Sensing 14: 5551, 2022.
- 596 Esch T, Heldens W, Hirner A, Keil M, Marconcini M, Roth A, Zeidler J, Dech S, Strano E.: Breaking new ground in
- 597 mapping human settlements from space The Global Urban Footprint. ISPRS Journal of Photogrammetry and Remote
- **598** Sensing 134: 30-42, 2017.
- 599 GADM 4.1. https://gadm.org/.
- 600 GDAL/OGR contributors.: GDAL/OGR Geospatial Data Abstraction software Library. Open Source Geospatial Foundation.
- 601 https://gdal.org, 2024.
- 602 Hirabayashi Y, Mahendran R, Koirala S, Konoshima L, Yamazaki D, Watanabe S, Kim H, Kanae S.: Global flood risk under
- 603 climate change. Nature climate change 3: 816-821, 2013.
- 604 Huizinga J, De Moel H, Szewczyk W.: Global flood depth-damage functions: methodology and the database with guidelines.
- 605 European Commission, Joint Research Centre, 2016.
- 606 Iizumi T, Takikawa H, Hirabayashi Y, Hanasaki N, Nishimori M.: Contributions of different bias-correction methods and
- 607 reference meteorological forcing data sets to uncertainty in projected temperature and precipitation extremes. Journal of
- 608 Geophysical Research-Atmospheres, 2017.
- 609 IMF.: How Should We Measure City Size Theory and Evidence Within and Across Rich and Poor Countries. IMF:
- 610 Washington, DC, USA.
- 611 https://www.imf.org/en/Publications/WP/Issues/2019/09/20/How-Should-We-Measure-City-Size-Theory-and-Evidence-With
- 612 in-and-Across-Rich-and-Poor-Countries-48671, 2019.
- 613 Inoue S.: Agriculture and its Policy in Thailand. MAFF (Ministry of Agriculture, Forestry and Fisheries).
- 614 https://www.maff.go.jp/primaff/koho/seminar/2010/attach/pdf/101026 01.pdf. (In Japanese), 2010.
- 615 IPCC.: Managing the Risks of Extreme Events and Disasters to Advance Climate Change Adaptation. A Special Report of
- 616 Working Groups I and II of the Intergovernmental Panel on Climate Change: 582 pp. 2012.
- 617 Jongman B, Kreibich H, Apel H, Barredo JI, Bates PD, Feyen L, Gericke A, Neal J, Aerts JCJH, Ward PJ.: Natural Hazards
- **618** and Earth System Sciences 12: 3733-3752, 2012.
- 619 Jovel RJ, Mudahar M.: Damage, loss, and needs assessment guidance notes: Volume 3. Estimation of post-disaster needs for
- 620 recovery and reconstruction. Washington, DC, Report. http://hdl.handle.net/10986/19046, 2010.
- 621 Kimura S, Ishikawa Y, Katada T, Asano K, Sato H.: The structural analysis of economic damage of offices by flood disasters
- 622 in urban areas. Japanese Journal of JSCE 63: 88-100 (in Japanese), 2007.

- 623 Koks EE, Bočkarjova M, De Moel H, Aerts JCJH.: Integrated Direct and Indirect Flood Risk Modeling: Development and
- 624 Sensitivity Analysis; Integrated Direct and Indirect Flood Risk Modeling, Risk Analysis 35: 882-900, 2015.
- 625 Kummu M, Maija T, Guillaume JHA.: Gridded global datasets for gross domestic product and human development index
- 626 over 1990–2015. Scientific Data 5: 180004, 2018.
- 627 Kummu, M., Kosonen, M., & Masoumzadeh Sayyar, S.: Downscaled gridded global dataset for gross domestic product
- **628** (GDP) per capita PPP over 1990–2022. Scientific Data, 12(1), 178, 2025.
- 629 Ministry of Economy, Trade, and Industry.: A survey on industry statistics.
- 630 https://www.meti.go.jp/statistics/tyo/kougyo/result-2/h10/kakuho/youti/youti1.html, 2007.
- 631 Ministry of Land, Infrastructure, Transport and Tourism.: Mesh Data of Subdivided Land Use in Urban Area.
- 632 https://nlftp.mlit.go.jp/ksj/gml/datalist/KsjTmplt-L03-b-u.html, 2021.
- 633 Morikawa M. Economies of density and productivity in service industries: An analysis of personal service industries based
- 634 on establishment-level data. Review of Economics and Statistics 93: 179–192, 2011.
- 635 Murakami, D., & Yamagata, Y.: Estimation of gridded population and GDP scenarios with spatially explicit statistical
- **636** downscaling. Sustainability, 11(7), 2106, 2019.
- 637 NESDC (Office of the National Economic and Social Development Council, Thailand).: Gross Provincial Product
- 638 1995–2009 (16 sectors). https://www.nesdc.go.th/main.php?filename=gross_regional, 2016.
- 639 Pesaresi M, Politis P.: GHS-BUILT-S R2022A: GHS built-up surface grid, derived from Sentinel2 composite and Landsat,
- 640 multitemporal (1975–2030). European Commission, Joint Research Centre (JRC), 2022.
- 641 Potapov P, Svetlana T, Matthew CH, Alexandra T, Viviana Z, Ahmad K, Xiao-Peng S, Amy P, Quan S, Jocelyn C.: Global
- 642 maps of cropland extent and change show accelerated cropland expansion in the twenty-first century. Nature Food 3: 19–28,
- **643** 2022.
- 644 Rose A.: Economic Principles, Issues, and Research Priorities in Hazard Loss Estimation. Modeling Spatial and Economic
- 645 Impacts of Disasters, Springer Berlin Heidelberg, Berlin, Heidelberg; 13-36, 2004.
- 646 Ru, Y., Blankespoor, B., Wood-Sichra, U., Thomas, T. S., You, L., & Kalvelagen, E.: Estimating local agricultural GDP
- 647 across the world. Earth System Science Data Discussions, 2022, 1-36, 2022.
- 648 Shoji T, Yamazaki D, Kita Y, Megumi W.: Global Sectoral GDP map at 30" resolution (SectGDP30) v1.0,
- 649 https://doi.org/10.5281/zenodo.13991673, 2024.
- 650 Sieg T, Thomas S, Kristin V, Reinhard M, Bruno M, Heidi K.: Integrated assessment of short-term direct and indirect
- 651 economic flood impacts including uncertainty quantification. PLOS ONE 14: e0212932, 2019.
- 652 Taguchi R, Tanoue M, Yamazaki D, Hirabayashi Y.: Global-scale assessment of economic losses caused by flood-related
- 653 business interruption. Water 14: 967, 2022.
- 654 Tanoue M, Hirabayashi Y, Ikeuchi H.: Global-scale river flood vulnerability in the last 50 years. Scientific Reports 6: 36021,
- **655** 2016.

- 656 Tanoue M, Taguchi R, Nakata S, Watanabe S, Fujimori S, Hirabayashi Y.: Estimation of direct and indirect economic losses
- 657 caused by a flood with long-lasting inundation: Application to the 2011 Thailand flood. Water Resources Research 56, 2020.
- 658 Tanoue M, Taguchi R, Alifu H, Hirabayashi Y.: Residual flood damage under intensive adaptation. Nature Climate Change
- **659** 11: 823-826, 2021.
- 660 Tellman B, Sullivan JA, Kuhn C, Kettner AJ, Doyle CS, Brakenridge GR, Erickson TA, Slayback DA.: Satellite imaging
- 661 reveals increased proportion of population exposed to floods. Nature 596: 80–86, 2021.
- 662 The European Environmental Agency.: CORINE Land Cover.
- 663 https://land.copernicus.eu/en/products/corine-land-cover?tab=main, 2017.
- 664 Theobald DM.: Development and Applications of a Comprehensive Land Use Classification and Map for the US. PLoS
- 665 ONE 9: e94628, 2014.
- 666 Wenz L, Carr RD, Kögel N, Kotz M, Kalkuhl M.: DOSE Global data set of reported sub-national economic output. Sci
- 667 Data 10: 425, 2023.
- 668 Wenz L, Willner SN.: 18. Climate impacts and global supply chains: An overview. Handbook on Trade Policy and Climate
- 669 Change, 290, 2022.
- 670 Willner SN, Otto C, Levermann A.: Global economic response to river floods. Nature Climate Change 8: 594–98, 2018.
- 671 The World Bank.: 2011 Thailand Floods: Rapid Assessment for Resilient Recovery and Reconstruction Planning.
- 672 https://recovery.preventionweb.net/publication/2011-thailand-floods-rapid-assessment-resilient-recovery-and-reconstruction-
- 673 planning, 2011.
- 674 The World Bank.: World Development Indicators. https://databank.worldbank.org/source/world-development-indicators,
- **675** 2023.
- 676 Yamazaki, D, Kanae S, Kim H, Oki T.: A physically-based description of floodplain inundation dynamics in a global river
- 677 routing model: FLOODPLAIN INUNDATION DYNAMICS. Water Resources Research 47: w04501, 2011.
- 678 Zhuang, L., & Ye, C.: More sprawl than agglomeration: The multi-scale spatial patterns and industrial characteristics of
- 679 varied development zones in China. Cities, 140, 104406, 2023